ELSEVIER

Thermochimica Acta 361 (2000) 97–111

thermochimica acta

www.elsevier.com/locate/tca

Investigation of isothermal curing of a thermosetting system by temperature-modulated differential scanning calorimetry: information derived from the phase shift and the determination of the complex heat capacity

J.E.K. Schawe

Mettler Toledo GmbH, Sonnenbergstr. 74, CH-8603 Schwerzenbach, Switzerland

Received 7 January 2000; received in revised form 3 April 2000; accepted 4 April 2000

Abstract

Isothermal curing of a thermosetting system was investigated by temperature-modulated differential scanning calorimetry (TMDSC) at different frequencies. From the periodic component of the heat flow, the amplitude and the phase shift were determined. The amplitude mainly delivers information on the thermal relaxation (vitrification process), whereas the phase shift also includes information of the temperature dependence of the reaction rate and the heat transfer conditions. A procedure is introduced to separate these effects. As a result, we get the phase shift that is only due to the thermal relaxation. This is required to determine the correct complex heat capacity. Additionally, the phase shift delivers information on the reaction kinetics, i.e. the change from chemical-controlled to diffusion-controlled kinetics. © 2000 Elsevier Science B.V. All rights reserved.

Keywords: Thermosetting systems; Curing; Reaction kinetics; Vitrification; Complex heat capacity; Temperature-modulated DSC

1. Introduction

In the past, extensive calorimetric investigation has been performed to get a better understanding of the curing reaction of different thermosetting systems [1–3].

During curing, the glass transition temperature increases due to network formation. If the glass transition region of the reacting polymer network reaches the curing temperature, vitrification occurs, the cooperative molecular motions start freezing and the reaction becomes a diffusion-controlled one, i.e. vitrification can be described as a chemically induced transition from a liquid (or rubbery) state to the glassy state which is usually accompanied by a change in the heat capacity. The vitrification process can be described in analogy to the glass transition as a thermal relaxation process [4]. Using the conventional differential scanning calorimetry (DSC) technique, the heat capacity change related to the vitrification is masked by the relatively large exothermal reaction peak. Gobrecht et al. [5] proposed the temperature-modulated differential scanning calorimetry (TMDSC) technique to investigate such heat capacity changes during chemical reactions. In the case of isothermal curing of thermosetting systems, a practical realization has been presented in [6–8]. Their measurements show a vitrification transition with

E-mail address: juergen.schawe@mt.com (J.E.K. Schawe).

PII: S0040-6031(00)00551-7

Nomenclature

a	constant factor
A	proportionality factor
b	constant factor
B	proportionality factor
c	heat capacity
c^*	complex heat capacity
c'	real part of the complex heat capacity
c''	imaginary part of the complex heat capacity
$\|c\|$	modulus of the complex heat capacity
$\langle c_{10} \rangle$	average value of $\|c\|$ measured at 10 ks
c_a^*	apparent complex heat capacity
c_a'	real part of the apparent complex heat capacity
c_a''	imaginary part of the apparent complex heat capacity
$\|c_a\|$	modulus of the apparent complex heat capacity
c_{dyn}	dynamic heat capacity
c_{dyn}'	real part of the dynamic heat capacity
c_{dyn}''	imaginary part of the dynamic heat capacity
$\dot{c}_{dyn}$	time derivative of the dynamic heat capacity
c_{st}	static heat capacity
E	activation energy
f	frequency
$f(\xi)$	conversion function
F_1	first correction function (influence of the chemical-controlled reaction)
F_2	second correction function (influence of the heat capacity change)
F_3	third correction function (influence of the diffusion-controlled reaction)
i	imaginary unit
k	rate constant
k_0	pre-exponential factor
K	calibration factor of the heat flow amplitude
m	sample mass
Q	heat
R	gas constant
t	time
t_1	time of the exothermal maximum in the underlying heat flow
t_2	time before vitrification
t_3	time after vitrification
t_4	minimum time of φ_2-curve
t_p	modulation period
t_v	vitrification time
T	temperature
T_a	temperature amplitude
T_{cur}	curing temperature

Greek symbols

β	heating rate
δT	temperature perturbation
Δc	change in the heat capacity during vitrification
Δh_r	specific enthalpy of reaction
Φ	heat flow
Φ_a	heat flow amplitude
Φ_p	periodic component of the heat flow
Φ_u	underlying component of the heat flow
φ	phase shift due to relaxation
φ_1	phase shift after the first correction (influence of the chemical-controlled reaction)
φ_2	phase shift after the second correction (influence of the heat capacity change)
φ_{HT}	phase shift due to heat transfer
φ_{cal}	calibrated phase shift
φ_d	phase shift due to a diffusion-controlled reaction
φ_m	measured phase shift
$\varphi_{\Delta c}$	phase shift due to change in the heat capacity
φ_ξ	phase shift due to a chemical-controlled reaction
v	rate of reaction
v_c	rate of the chemical-controlled reaction
v_d	rate of the diffusion-controlled reaction
τ	relaxation time
ω	angular frequency
ξ	degree of reaction (conversion)

characteristic stepwise decreases in the heat capacity. Van Mele and coworkers used this information to model the change in the reaction kinetics from a chemical-controlled reaction to a diffusion-controlled one [9]. For this procedure, only the underlying heat flow and the amplitude of the periodic component of the heat flow are necessary.

An additional information delivered by the TMDSC technique is the phase shift, which allows the determination of the complex heat capacity ($c^* = c' - ic''$) during isothermal curing [9–13]. The real part of the complex heat capacity, c', describes the normal heat capacity. The imaginary part c'' shows a peak during reaction. The interpretation of this peak is still controversial. Some authors claim that this peak is due to relaxation effects [10,11]. Others find it is linked to kinetic events [9].

Because the phase shift is rather small, it affects mostly c''. Therefore, a correct determination and interpretation of c'' requires detailed knowledge of the nature of the phase shift. It has been shown that the phase shift measured by TMDSC depends on different properties such as heat transfer [14], heat capacity change and thermal contact [15] and the rate of the chemical reaction [16]. In this paper, we discuss these influences exemplarily on the isothermal curing of diglycidylether of bisphenol A (DGEBA) cross-linked with diaminodiphenyl methane (DDM). The results are: (i) a procedure for determination of the complex heat capacity; (ii) measurements of the frequency dependence of the complex heat capacity during vitrification; (iii) additional information on the change in the reaction kinetics.

2. Experimental

Commercial DGEBA (Shell Chemical, Epikote 828) and DDM (Aldrich) were used as a thermosetting system. The substances were poured together in the stoichiometric amounts of 2 mol% DGEBA and 1 mol% DDM and heated up to 120°C for 20 s. During this time, the sample was stirred to get a homogeneous mixture. The mixture was then rapidly cooled to room temperature and 25 specimens with 3.0(±0.3) mg in aluminum crucibles were prepared. The samples were stored at −35°C and measured during the next 5 days. To check the chemical stability of the samples during this period, one sample per day was measured by DSC at 10 K/min. The glass transition temperature (−14.8°C), the heat of reaction (410 J/g) and the temperature of the reaction peak maximum (160°C) were determined. During this time, no significant deviations of these properties could be measured.

The measurements were performed on a Mettler Toledo DSC 821[e] with intracooler using the ADSC software option for temperature modulation. The instrument was temperature-calibrated with water, indium and tin. The onset temperature of the melting peaks were measured at 0.5, 1, 2, 5 and 10 K/min. The measured onset temperature is a linear function of the heating rate with the slope τ_{lag}. The extrapolated onset temperature (to zero heating rate) was used for calibration [17,18]. For the TMDSC measurements, τ_{lag} [19] was set to 0. Indium was used for the heat flow calibration. The furnace atmosphere was defined by 50 ml/min nitrogen.

Before the measurement, the DSC furnace was heated to the curing temperature (T_{cur}=100°C). For maximum reproducibility, the sample was placed in the furnace using a sample robot, but the sample was kept at room temperature for a period no longer than 2 min before measurement. In the TMDSC measurements, a temperature amplitude T_a of 0.5 K was used. The period t_p was 12, 24, 48, 60, 96 or 210 s, respectively. The measuring time was approximately 10 ks. An empty pan was run under the same condition for reference. For all calculations, blank corrected data (sample run subtracted by empty pan run) were used.

3. Description of the signals

For a better understanding, a list of the symbols used is given at the end of the article.

3.1. Heat flow and complex heat capacity

If a sinusoidal furnace temperature perturbation is used, the related response of the heat flow to the sample is described by an amplitude and a phase shift. Both parameters are influenced by the heat transfer conditions within the sample and the sample holder (furnace and sensor) [14]. The modulus of the complex heat capacity is determined from the amplitudes of the temperature T_a and the heat flow Φ_a:

$$|c| = \frac{K}{m}\frac{\Phi_a}{T_a\omega} \quad (1)$$

where K is a calibration factor [14,20], m the sample mass and ω ($=2\pi f=2\pi/t_p$) is the angular frequency.

Correcting the influence of heat transfer, φ_{HT}, from the measured phase shift φ_m gives

$$\varphi_{cal} = \varphi_m - \varphi_{HT} \tag{2}$$

where φ_{cal} is the calibrated phase shift. This signal can be used to determine a frequency dependent apparent complex heat capacity $c_a^*(\omega)=c_a'(\omega)-ic_a''(\omega)$. The real and imaginary parts are $c_a'=|c|\cos\varphi_{cal}$ and $c_a''=|c|\sin\varphi_{cal}$, respectively.

In the case of curing, two time dependent processes take place simultaneously. The first process is the chemical reaction, which can be described by the temperature- and time-dependent degree of reaction (conversion) $\xi(T, t)$. Secondly, sample vitrifies during reaction, which can be described as thermal relaxation [11]. For a sufficiently small temperature perturbation δT, the periodic part of the sample response can be linearized [21–24]. In this case, it is useful to introduce a time-dependent generalized heat capacity [25]:

$$c(t,T) = c_{st}(T) + c_{dyn}(t,T) \tag{3}$$

The static part c_{st} is determined by the fast modes of the molecular motions which are always in equilibrium. This part is temperature dependent and equals the heat capacity defined in reversible thermodynamics (c_p). The dynamic heat capacity c_{dyn} describes the time dependent relaxation processes due to the internal degrees of freedom with a distinct time dependence during the experiment.

For the quasi-isothermal curing experiment, the sample temperature is

$$T(t) = T_{cur} + \delta T(t) = T_{cur} + T_a \sin\omega t \tag{4}$$

where T_{cur} is the curing temperature and T_a the temperature amplitude. The heating rate is then

$$\beta(t) = T_a\omega\cos\omega t \tag{5}$$

If Δh_r is the specific enthalpy of the curing reaction and m the sample mass, the normalized heat of the sample reads

$$\frac{Q(t,T)}{m} = \Delta h_r\xi(t) + \frac{\partial c(T,t)}{\partial T}[\delta T(t)]^2 + \frac{d}{dt}\int_0^t c(t')\delta T(t-t')dt' \tag{6}$$

The first term in Eq. (6) describes the heat of reaction, the second term is due to the temperature dependence of the heat capacity and the third term represents the relaxation process (vitrification). The partial derivative of Eq. (6) is the calibrated heat flow:

$$\begin{aligned}\frac{\Phi(t)}{m} &= \Delta h_r v(t) + \Delta h_r\frac{\partial v(t)}{\partial T}\delta T(t) + 2\frac{\partial c}{\partial T}\delta T\beta(t) + c_{st}\beta(t) + \int_0^t \dot{c}_{dyn}(t')\beta(t-t')dt' \\ &= \Delta h_r v(t) + \left[c_{st}\beta + \Delta h_r\frac{\partial v(t)}{\partial T}\delta T + \int_0^t \dot{c}_{dyn}(t')\beta(t-t')dt'\right] + 2\frac{\partial c}{\partial T}\delta T\beta\end{aligned} \tag{7}$$

where $v = d\xi/dt$ is the rate of reaction.

In Eq. (7), the part in the square brackets describes the periodic component of the calibrated heat flow. The first summand is the component of the underlying signal component due to the isothermal chemical. The term $2(\partial c/\partial T)\delta T\beta$ corresponds to a non-linear sample response. For thermal relaxation, it can be neglected in case of small temperature amplitudes (less than 1 K) [23].

An additional non-linear effect is expected as a result of the non-linear temperature- and time dependence of the reaction rate. For sufficiently small temperature amplitudes and short periods, the reaction rate can be linearized in the related time and temperature intervals. Therefore, in agreement with experimental results, such non-linear effects can be neglected for the present data evaluation.

For a sinusoidal temperature perturbation, the convolution integral in Eq. (7) is [26]

$$\int_0^t \dot{c}_{dyn}(t')\beta(t-t')dt' = \omega T_a(c_{dyn}'(\omega)\cos\omega t + c_{dyn}''(\omega)\sin\omega t)$$

Inserting Eqs. (4) and (5) into Eq. (7) and combining the above facts delivers

$$\frac{\Phi(t)}{m} = \Delta h_r v(t) + \left[\omega T_a(c_{st} + c_{dyn}'(\omega))\cos\omega t + \omega T_a\left(\frac{\Delta h_r}{\omega}\frac{\partial v(t)}{\partial T} + c_{dyn}''(\omega)\right)\sin\omega t\right] \tag{8}$$

The underlying component of the heat flow, Φ_u, can be evaluated by moving averaging the modulated heat flow over one period. The periodic component $\Phi_p=\Phi-\Phi_u$ can be separated into a sinus and a cosine part. Fourier analysis of Φ_p delivers the respective

amplitudes and division by ωT_a yields the apparent complex heat capacity:

$$c_a^*(\omega) = c_a'(\omega) - ic_a''(\omega) = (c_{st} + c_{dyn}'(\omega)) - i\left(\frac{\Delta h_r}{\omega}\frac{\partial v}{\partial T} + c_{dyn}''(\omega)\right) \quad (9)$$

In this particular case, the imaginary part of the apparent complex heat capacity is also influenced by the temperature dependence of the rate of reaction. This is the difference between the apparent complex heat capacity $c_a^*(\omega)$ and the complex heat capacity $c^*(\omega)$:

$$c^*(\omega) = c'(\omega) - ic''(\omega) = (c_{st} + c_{dyn}'(\omega)) - ic_{dyn}''(\omega) \quad (10)$$

3.2. Phase shift and amplitude of the heat flow rate

An alternative formulation of the periodic component of the heat flow rate is

$$\Phi_p(t) = \Phi_a(t)\cos(\omega t - \varphi_m(t)) \quad (11)$$

with the amplitude

$$\Phi_a(t) = K\omega m T_a \sqrt{(c_{st}(t) + c_{dyn}'(\omega,t))^2 + \left(\frac{\Delta h_r}{\omega}\frac{\partial v(t)}{\partial T} + c_{dyn}''(\omega,t)\right)^2} \quad (12)$$

and the phase shift

$$\tan(\varphi_m(t) - \varphi_{HT}) = \frac{1}{c_{st}(t) + c_{dyn}'(\omega,t)} \times \left(\frac{\Delta h_r}{\omega}\frac{\partial v(t)}{\partial T} + c_{dyn}''(\omega,t)\right) \quad (13)$$

K is the calibration factor of the heat flow amplitude and φ_{HT} the phase shift due to heat transfer. The square root in Eq. (12) is the modulus of the apparent complex heat capacity $|c_a|$.

Neglecting the relaxation process, Eqs. (12) and (13) correspond to a chemical reaction model proposed by Lacey et al. [16].

4. Results and discussion

4.1. Calibration of amplitude and phase shift

The underlying heat flow, the heat flow amplitude and the measured phase shift are shown in Fig. 1 for the measurement with t_p=60 s. The phase shift shows a negative peak which corresponds to the maximum

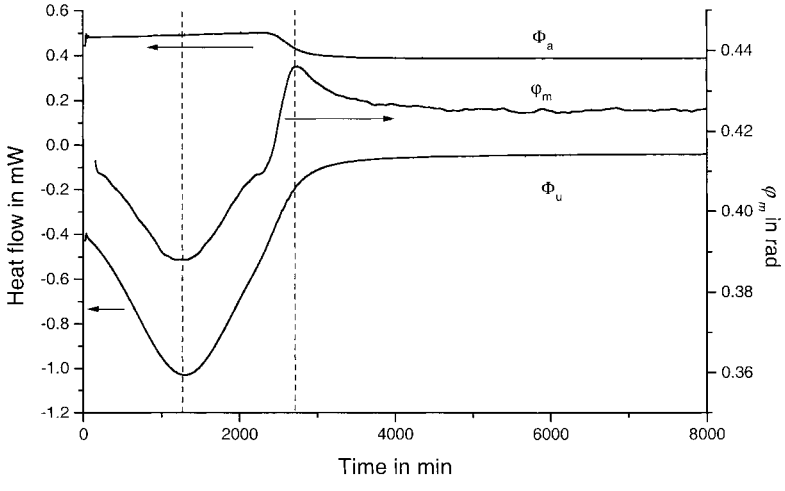

Fig. 1. Underlying heat flow Φ_u, heat flow amplitude Φ_a and measured phase shift φ_m as a function of curing time. The modulation period is 60 s. The exothermal direction is downwards.

reaction rate (the maximum time of the exothermal reaction in the underlying heat flow). The positive peak of the phase shift correlates with the stepwise decrease in the heat flow amplitude.

The underlying component Φ_u is properly calibrated due to the heat flow calibration. However, the amplitude Φ_a and the phase shift φ_m are affected by the K and φ_{HT}, respectively (see Eqs. (1) and (2)), which have to be calibrated.

The calibration factor of the amplitude K depends on the frequency or period [14]. With increasing frequency, K decreases because the heat transfer conditions get more and more important. For large periods viz. $t_p \geq 60$ s, K is approximately unity. With higher frequencies, K first decreases slowly (for t_p=48 and 24 s, K is in the order of 0.95 and 0.8, respectively) and then rapidly (K at t_p=18 s is around 0.5).

The calibration procedure for the amplitudes was as follows: for periods larger than 48 s, K was set to unity and the modulus of the apparent complex heat capacity was calculated using Eq. (12). Outside the transition region, all curves (t_p=60, 96, 210 s) fit very well together (Fig. 2). From these three curves, the average value $\langle c_{10} \rangle$ at 10 ks was calculated. For the other measurements (t_p=48, 24, 18 s), the apparent complex heat capacity was calculated in the same way as in the first case. Then, K was determined as the quotient of $\langle c_{10} \rangle$ and the value of the actual curve at t=10 ks. The calibrated curves are shown in Fig. 2.

φ_{HT} is a part of the contribution to the phase shift due to heat transfer. Formally, φ_{HT} can be split into four different parts, which are determined by the asymmetry of the sample holder, the heat transfer conditions inside the sample holder, the heat contact between sensor and sample and the heat transfer within the sample. Assuming that the heat contact and the sample thickness are approximately constant during an experiment, φ_{HT} is a constant and can be determined in intervals of the measured curves without relevant changes in the sample.

After a sufficiently long time (t>6 ks), the curing reaction is more or less terminated and the sample is in a quasi-stable state (in the time scale of the experiment). Therefore, the phase shift is only determined by the heat transfer φ_{HT}. Hence, to calibrate the phase shift, we assign $\varphi_{HT}=\varphi_m$ (t=10 ks). The calibrated phase shift curve $\varphi_{cal}(t)$ was determined by subtracting φ_{HT} from the measured phase shift curve $\varphi_m(t)$. The results are shown in Fig. 3. While the calibrated phase shift measured at t_p=18 s has a step around 2.4 ks, all other curves show a peak with a minimum around 1.2 ks. The amplitude of this peak decreases with the period. The phase shift at t_p=24 s shows a small maximum around 2.5 ks. Obviously, the calibrated phase shift is affected by different processes. One can use φ_{cal} for calculating the apparent complex heat capacity c_a^*. As discussed hereafter, some corrections are necessary for the determination of c^*.

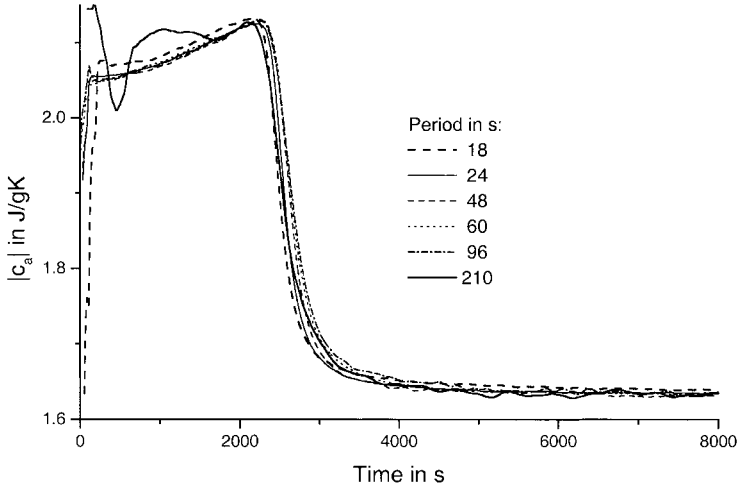

Fig. 2. The calibrated modulus of the apparent complex heat capacity measured by different periods.

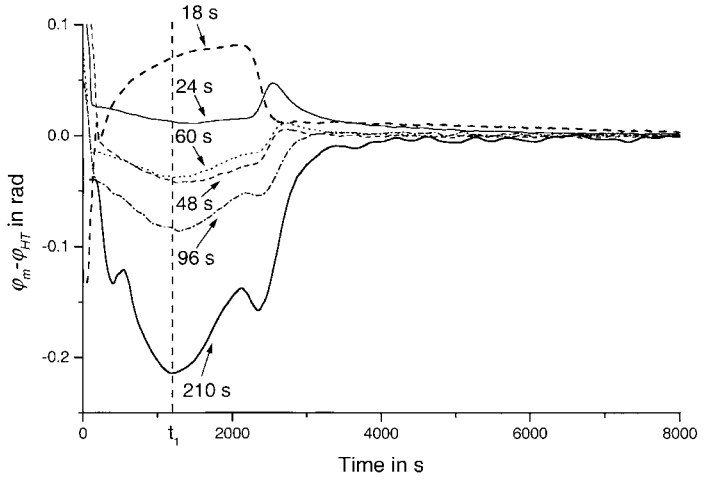

Fig. 3. Calibrated phase shift measured at different modulation periods by subtraction of φ_{HT}. The dotted line represents the time of the maximum reaction rate (maximum of the exothermal reaction in the underlying heat flow).

4.2. Basics of the correction of the phase shift

As mentioned above, φ_{cal} is influenced by thermal events of the sample and may be described by

$$\varphi_{cal} = \varphi + \varphi_\xi + \varphi_{\Delta c} \tag{14}$$

where φ is the phase shift due to thermal relaxation, φ_ξ denotes the influence of the chemical reaction and $\varphi_{\Delta c}$ takes into account the phase shift due to change in the heat capacity during reaction.

Correction of the phase shift means a separation of the different components φ, φ_ξ and $\varphi_{\Delta c}$. Due to the fact that $\varphi_{cal}<0.25$ rad, we can approximate $\tan x = x$. Therefore, it follows from Eqs. (13) and (14) that

$$\varphi(t) = \frac{c''(\omega,t)}{c'(\omega,t)} \tag{15}$$

and

$$\varphi_\xi(t) = \frac{1}{c'(\omega,t)} \frac{\Delta h_r}{\omega} \frac{\partial v(t)}{\partial T} \tag{16}$$

Because φ is relatively small, $c' \approx |c_a|$ is a good approximation in Eq. (16). Within experimental errors, we can replace the time-dependent reciprocal heat capacity in Eq. (16) by a constant factor $a = 1/|c_a|(t=1200\text{ s})$. Thus, the phase shift component due to chemical reaction reads

$$\varphi_\xi(t) \approx a \frac{\Delta h_r}{\omega} \frac{\partial v(t)}{\partial T} \tag{17}$$

The influence of the heat capacity change on the phase shift is discussed in detail in [15]. It is shown that

$$\varphi_{\Delta c}(t) = b\omega\,\Delta c \tag{18}$$

is a good approximation, where b is a constant due to heat transfer and $\Delta c = |c_a|(t\to\infty) - |c_a|(t)$. Considering Eqs. (14), (17) and (18), the calibrated phase shift can be expressed as

$$\begin{aligned}\varphi_{cal}(t) &= \varphi_m(t) - \varphi_{HT} \\ &= \varphi(t) + A t_p \frac{\partial v(t)}{\partial T} + B \frac{1}{t_p} \Delta c(t) \\ &= \text{term } 1 + \text{term } 2 + \text{term } 3\end{aligned} \tag{19}$$

where $A = a\,\Delta h_r/(2\pi)$ and $B = 2\pi b$.

To calculate the phase shift of the relaxation φ, the last two terms in Eq. (19) must be determined. These terms are a function of the period t_p, with the component due to the reaction being proportional to t_p and the component due to the heat capacity change being proportional to $1/t_p$. Thus, φ_ξ disappears for small periods ($\varphi_\xi(t_p=0)=0$) and $\varphi_{\Delta c}$ can be neglected for large periods ($\varphi_{\Delta c}(t_p\to\infty)=0$). In addition, φ is relatively small. Therefore, for large periods, the calibrated phase shift is mainly determined by φ_ξ ($\varphi_{cal}(t_p\to\infty) \approx \varphi_\xi$). One can use this relation for the phase shift correction if measurements at different periods are performed, as is shown below.

In Eq. (17), we assume that the phase shift due to the chemical reaction, φ_ξ, is independent of the sample

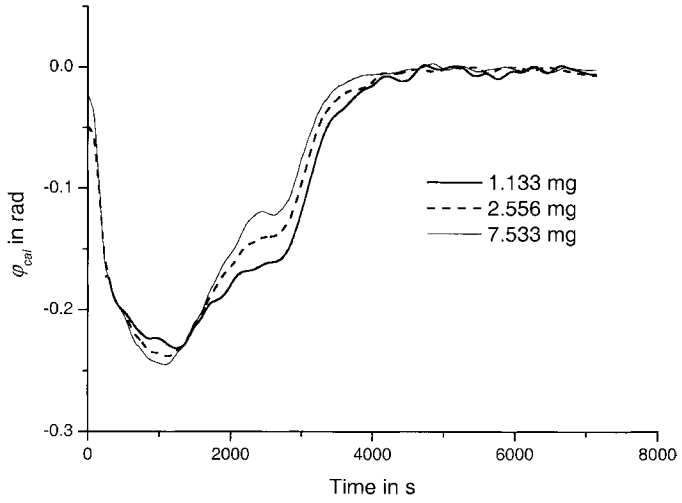

Fig. 4. The calibrated phase shift measured with different sample masses (t_p=210 s).

mass. In case of large periods (t_p=210 s), it is important for the presented procedure that the phase shift as a function of time is not influenced by sample parameters exempting the curing kinetics. This means that the influence of the transport of the exothermal heat of curing on φ_{cal} should be small or at least reproducible. Therefore, the sample mass was varied between 1.1 and 7.5 mg. Fig. 4 shows that the calibrated phase is sample mass independent within the experimental accuracy. This result was verified for t_p=48 s. As a result, a mass-dependent step in φ_{cal} can be measured. This step is due to the heat capacity change (cf. Eq. (18)) and increases with lower sample mass. This is consistent with the discussion in [15] because b is proportional to the reciprocal thermal conductivity of the heat transfer path between sample and sensor. The thermal conductivity increases with sample thickness. Also, for this period, the contribution of the phase shift imposed by the reaction is nearly mass-independent. However, to minimize any influences of the sample mass on the phase shift, the sample mass was approximately constant for all measurements.

4.3. The first correction of the influence of the reaction on the phase shift

Fig. 1 clearly shows that the peak in the phase shift around 1.2 ks follows the rate of reaction. The peak intensity increases with increasing period. This part of the phase shift curves is mainly influenced by φ_ξ. If

$$F_1(t) = A\frac{\partial v(t)}{\partial T} \tag{20}$$

is known, $B\,\Delta c(t)$ can be calculated from Eq. (19). Assuming that t_p=210 s is sufficiently large for this period, the φ_{cal}-curve around t_1 is equal to F_1 (t_1 is the time of exothermal maximum in Φ_u). Thus, $F_1(t_1)$ can be determined in the following manner:

1. Determination of φ_{cal} at time t_1 for all periods.
2. $F_1(t_1)$ is set to the calibrated phase shift at t_1 measured at t_p=210 s divided by the period: $F_1(t_1)=\varphi_{cal}(t_p=210\text{ s},\ t_1)/t_p$. The assumption is that, for such a large period, the calibrated phase shift in this region is only determined by the chemical reaction, neglecting the relatively small influence of the relaxation peak.
3. The component $\varphi_\xi(t_1)$ reduces to $\varphi_\xi(t_p,\ t_1)=F_1(t_1)t_p$.

The related diagram is shown in Fig. 5. This procedure requires a high accuracy of measurement for the period of 210 s. Therefore, this experiment was repeated three times and the average value was used for the calculations. F_1 at time t_1 is the result of this procedure.

To obtain the complete time-dependent function $F_1(t)$, information about the temperature dependence

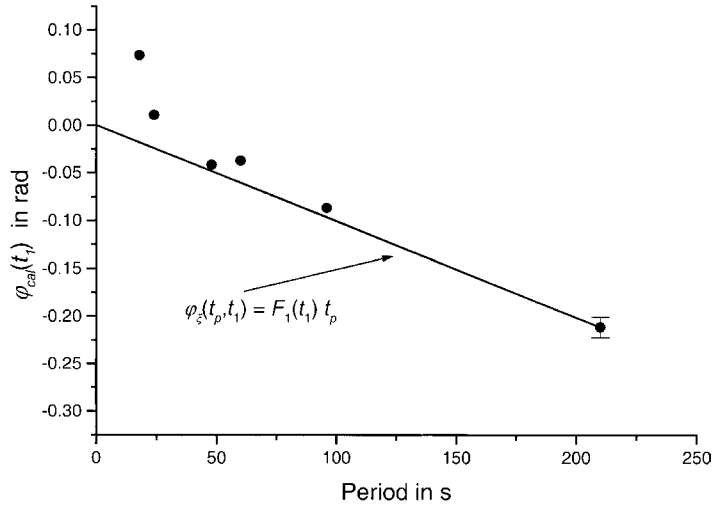

Fig. 5. Calibrated phase shift φ_{cal} at the time of the exothermal maximum of the underlying heat flow as a function of the period. The line represents the phase shift component induced by the chemical reaction φ_ξ. This line is determined by the coordinates (t_p=0, $\varphi_{cal}(t_1)$=0) and (t_p=210 s, $\varphi_{cal}(t_p, t_1)$).

of the reaction rate $\partial v(t)/\partial T$ is needed. Assuming that the reaction has only one reaction mechanism, the temperature dependence of the reaction rate is given by (see Appendix A)

$$\frac{\partial v(t)}{\partial T} \propto v(t) = \frac{\Phi_u(t)}{m\,\Delta h_r} \tag{21}$$

Thus, the correction function $F_1(t)$ can be written according to

$$F_1(t) = \frac{\Phi_u(t)}{\Phi_u(t_1)} F_1(t_1) \tag{22}$$

and the phase shift $\varphi_1(t)$ after this first correction reads

$$\varphi_1(t) = \varphi_{cal}(t) - F_1(t)t_p \tag{23}$$

Fig. 6 includes the resulting curves for all periods.

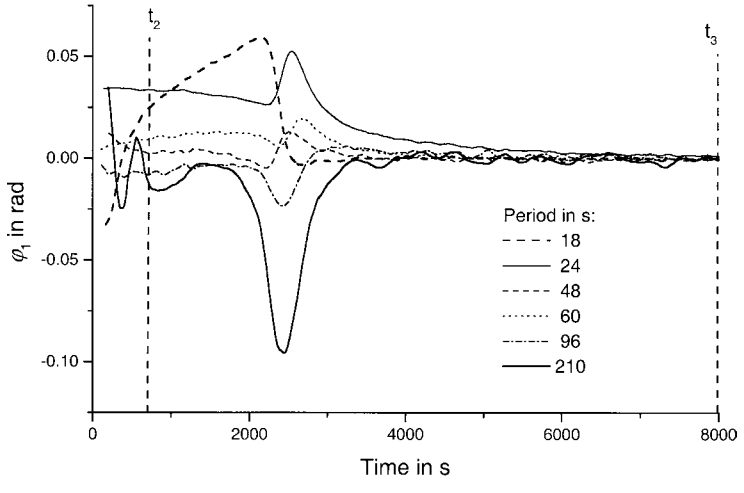

Fig. 6. The phase shift after the first correction for different periods (t_2=1.5 ks, t_3=8 ks).

4.4. The correction of the influence of the heat capacity change on the phase shift

Eq. (19) shows that the influence of the heat capacity change during reaction increases with decreasing period (term 3). This is in agreement with the results presented in Fig. 6. For example, at the curves for $t_p \leq 60$ s, the influence of the heat capacity change shows up in larger values of the phase shift at times before the step in the heat capacity.

The easiest way to estimate the correction function $F_2(t)$ for this second correction is to normalize the measured heat capacity functions $|c(t)|$ from Fig. 2:

$$F_2(t) = \frac{|c(t)| - |c(t_3)|}{|c(t_2)| - |c(t_3)|}(\varphi_1(t_2) - \varphi_1(t_3)) \tag{24}$$

The times t_2 and t_3 are selected at the beginning and end of the measurements as shown in Fig. 6. The phase shift after this (Δc-)correction is

$$\varphi_2(t) = \varphi_1(t) - F_2(t) \tag{25}$$

The result of the Δc-correction is shown in Fig. 7.

Two effects on the curves in Fig. 7 can be detected: first, a positive peak in the phase shift due to the thermal relaxation during vitrification (around 2.6 ks) for $t_p \geq 60$ s; second, a negative peak with a minimum at t_4=2.4 ks occurs. The intensity of this peak increases with the period. For large periods, only the negative peak is measured. In the case of shorter periods, a superposition of this negative peak and the relaxation peak appears.

The reason for the negative peak in the phase shift is the change in the reaction kinetics during curing.

4.5. Correction for the change in the reaction kinetics

The discussion in Appendix A shows that the correction of the reaction kinetics (Eq. (21)) is valid only if the curing reaction mechanism is constant. However, this is not true in reality. The glass transition shifts to higher temperatures during curing. If the glass transition temperature reaches the region of the curing temperature, the sample vitrifies and the reaction kinetics change from being chemical-controlled to diffusion-controlled [1]. This means that the activation energy by formal kinetic description changes during the reaction [27]. In this sense, the change in the curing reaction affects the phase shift. Therefore, Eq. (14) must be modified:

$$\varphi_{cal} = \varphi + \varphi_\xi + \varphi_{\Delta c} + \varphi_d \tag{26}$$

where φ_ξ and φ_d describe the influence of the chemical-controlled and the diffusion-controlled reaction, respectively. In the first and the second correction, φ_ξ and $\varphi_{\Delta c}$ are determined. Thus, the corrected phase shift φ_2 is

$$\varphi_2(t) = \varphi(t) + \varphi_d(t) \tag{27}$$

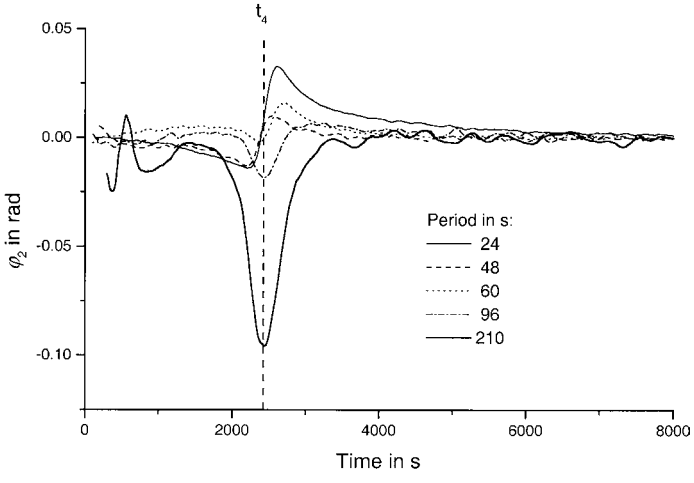

Fig. 7. The phase shift after the Δc-correction for different periods (t_4=2.4 ks).

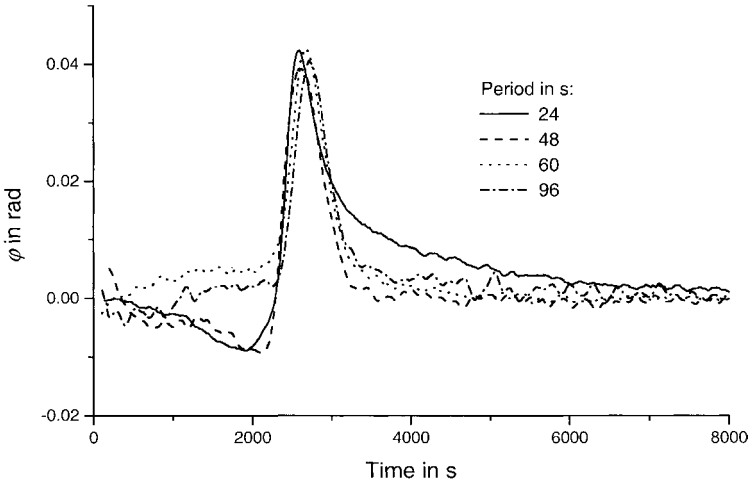

Fig. 8. The phase shift due to thermal relaxation (vitrification) during the curing reaction (corrected phase shift) measured for different periods.

Because φ_ξ and φ_d depend in the same way on the period, we assume that the phase shift at t_p=210 s is mostly determined by φ_d. In this case, we can apply a similar correction procedure as described in Section 4.3, i.e. we define the correction function F_3 using the phase shift measured for a period of 210 s:

$$F_3(t) = \frac{\varphi_2(t_p = 210\,s, t)}{t_p} \tag{28}$$

The corrected phase shift then equals

$$\varphi(t) = \varphi_2(t) - F_3(t)t_p \tag{29}$$

This is the phase shift now only due to the thermal relaxation processes. The results are shown in Fig. 8.

4.6. The complex heat capacity

From the results in Fig. 8, the real and the imaginary part of the complex heat capacity can determined by

$$c'(t_p, t) = |c_a(t_p, t)| \cos \varphi(t_p, t) \tag{30}$$

and

$$c''(t_p, t) = |c_a(t_p, t)| \sin \varphi(t_p, t) \tag{31}$$

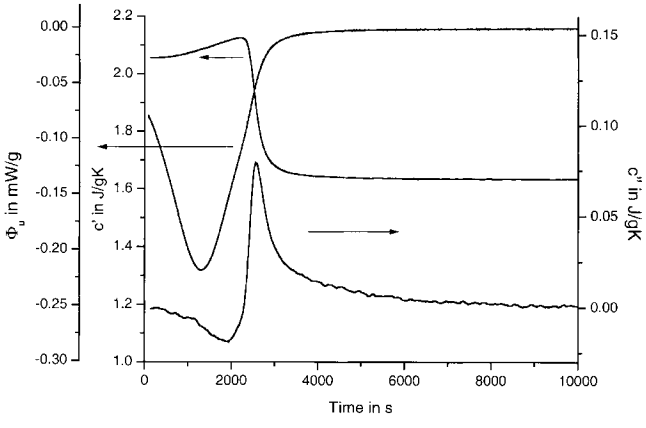

Fig. 9. The underlying heat flow rate and the real and the imaginary part of the complex heat capacity for t_p=24 s.

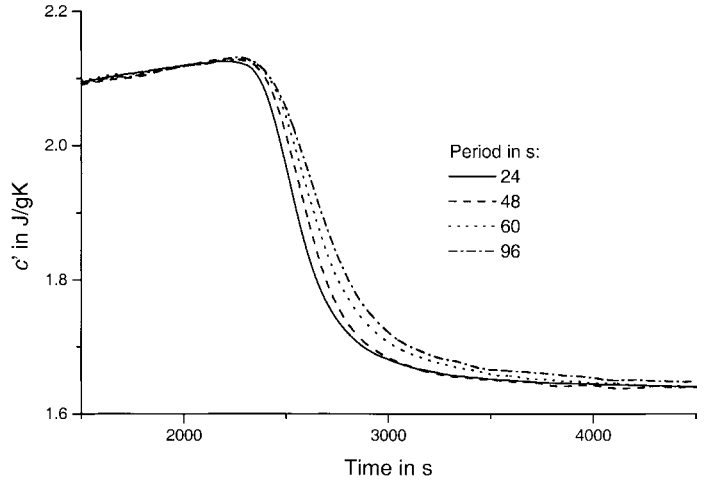

Fig. 10. The real part of the complex heat capacity measured with different periods.

For a period of 24 s, the underlying heat flow and the complex heat capacity are shown in Fig. 9. At a conversion of approximately 85%, the heat capacity drops from a value of the liquid state to the glassy heat capacity. The sample vitrifies, and as a consequence, the curing reaction slows down. The time of the peak maximum in the imaginary part of the complex heat capacity is the vitrification time t_v. This time corresponds to the inflection point of the c'-step. This is a typical appearance for a relaxation process. During relaxation processes, the signals are generally frequency-dependent. This is shown for the real and the imaginary part of the complex heat capacity in Figs. 10 and 11, respectively. With increasing period, the relaxation transition shifts to lower times. The characteristic relaxation time τ is defined by $\tau=t_p/2\pi$. The vitrification time dependence of τ (see Fig. 12) shows a good agreement with the results of dielectric measurement [28].

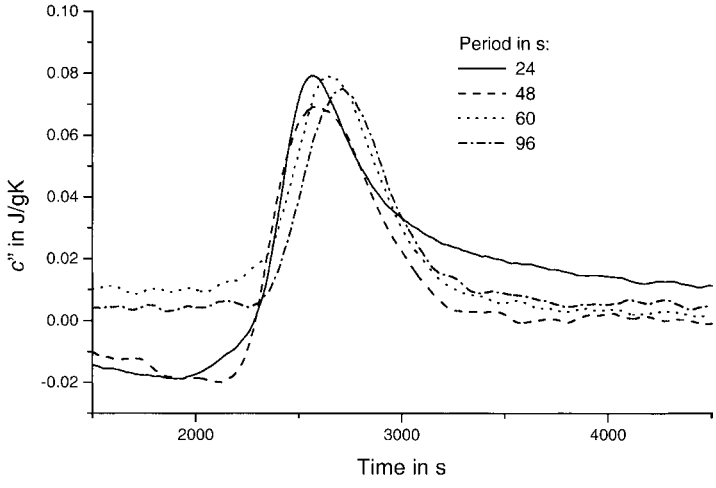

Fig. 11. The imaginary part of the complex heat capacity measured with different periods.

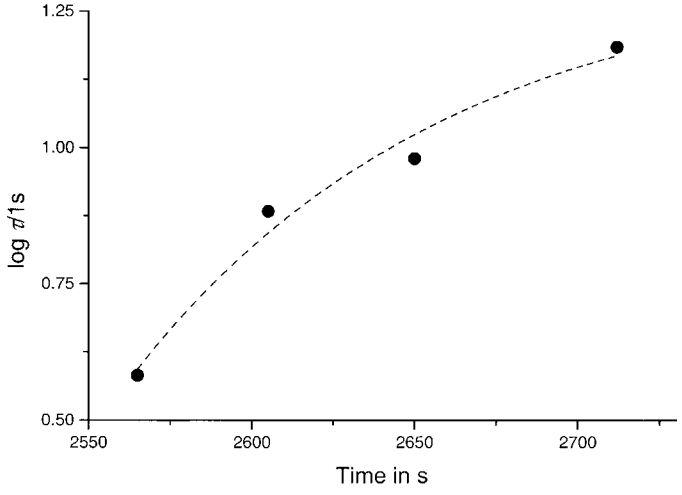

Fig. 12. The vitrification time dependence of the relaxation time due to vitrification.

4.7. Correspondences between phase shift and reaction kinetics

In the case of large periods, the calibrated phase shift curve can be described according to Eq. (19):

$$\varphi_{\mathrm{cal}}(t) = At_{\mathrm{p}}\frac{\partial v}{\partial T} \tag{32}$$

In the curve for t_{p}=210 s (Fig. 3), a large peak with a maximum at 1.2 ks is superimposed with a small peak. The maximum time for this is around 2.35 ks. For the correction procedure of the phase shift, we suggest an additive separation of the influence of the chemical-controlled and the diffusion-controlled reaction on the phase:

$$\varphi_{\mathrm{cal}}(t) = At_{\mathrm{p}}\left(\frac{\partial v_{\mathrm{c}}}{\partial T} + \frac{\partial v_{\mathrm{d}}}{\partial T}\right) \tag{33}$$

where $\partial v_{\mathrm{c}}/\partial T$ and $\partial v_{\mathrm{d}}/\partial T$ denote the temperature dependencies of the chemical-controlled and the diffusion-controlled reaction rate, respectively.

In Fig. 3, the second peak in the phase shift at 2.35 ks is an indication of the important temperature dependence of the diffusion-controlled reaction. Using the estimation

$$\frac{\partial v_{\mathrm{c}}}{\partial T} \propto \Phi_{\mathrm{u}} \tag{34}$$

a curve proportional to $\partial v_{\mathrm{d}}/\partial T$ can be estimated using large periods (see Fig. 6, curve t_{p}=210 s). This curve shows the first measurable influence of diffusion on the reaction at approximately 1.5 ks. For this assumption, the phase shift for large periods is applicable as an indication of the influence of diffusion on the curing reaction.

5. Conclusion

The vitrification transition during isothermal curing of a therosetting system is accompanied by a step-like decrease in the heat capacity and a change in the reaction kinetics due to diffusion. In a TMDSC experiment, the measured phase shift is affected by heat transfer, chemical reaction and relaxation. Because the various effects show different frequency dependencies, their separation from each other is possible. The correction procedure consists of four steps:

1. calibration of amplitude and phase shift;
2. first correction of the influence of the reaction rate on the phase shift. The assumption for this is that the underlying reaction rate is proportional to the temperature dependence of the reaction rate of the chemical-controlled reaction;
3. correction of the influence of the heat capacity change during the reaction on the phase shift using the normalized heat capacity curve;
4. second correction of the influence of the reaction rate, i.e. the influence of the change in the kinetics.

Using the corrected phase shift, the complex heat capacity c^* is determined and the frequency dependence of the vitrification time is measured.

Apart from the actual measurement, the procedure presented here required at least one additional measurement at a relatively large period. This additional measurement yields the information of the influence of the reaction on the phase shift. Measurements with large periods deliver additional information on the reaction kinetics. Thus, the outlined procedure allows a detailed analysis of the curing kinetics in thermosetting materials; it can be further developed for the analysis of different chemical reactions showing changes in the reaction kinetics.

Acknowledgements

The author would like to thank I. Alig (Deutsches Kunststoffinstitut, Darmstadt), R. Riesen and M. Schubnell (Mettler Toledo GmbH, Schwerzenbach) for helpful discussions.

Appendix A

Chemical reactions are usually described by

$$\frac{\partial \xi}{\partial t} = v = k(T) f(\xi) \tag{A.1}$$

where the conversion ξ is a function of the reaction time, k is the temperature-dependent rate constant and $f(\xi)$ is the conversion function which is a model function dependent on the reaction mechanism. According to the Arrhenius equation, the rate constant is given by

$$k(T) = k_0 \exp\left(-\frac{E}{RT}\right) \tag{A.2}$$

where k_0 is the pre-exponential factor, E the activation energy and R is the gas constant.

Since $f(\xi)$ is assumed to be independent of temperature, the temperature dependence of the reaction rate is

$$\frac{\partial v}{\partial T} = f(\xi) \frac{\mathrm{d}k}{\mathrm{d}T} \tag{A.3}$$

Inserting Eq. (A.2) in Eq. (A.3) delivers

$$\frac{\partial v}{\partial T} = \frac{E}{RT^2} f(\xi) k(T) = \frac{E}{RT^2} v \tag{A.4}$$

For a quasi-isothermal TMDSC experiment, the temperature T in Eq. (A.4) represents the constant curing temperature T_0 in Eq. (4). Furthermore, the reaction rate is proportional to the underlying heat flow:

$$\Phi_\mathrm{u}(t) = m \, \Delta h_\mathrm{r} \, v(t) \tag{A.5}$$

where m is the sample mass and Δh_r is the enthalpy of reaction. Combining Eqs. (A.4) and (A.5), we get

$$\frac{\partial v}{\partial T} = \frac{E}{RT^2} \frac{\Phi_\mathrm{u}}{m \, \Delta h_\mathrm{r}} \propto v \tag{A.6}$$

References

[1] K. Hori, H. Hiura, M. Sawada, I. Mita, H. Kambe, J. Polym. Sci. A 1 (8) (1970) 1357.
[2] S. Sourour, M.R. Kamal, Thermochim. Acta 14 (1976) 41.
[3] G. Wisanrakkit, J.K. Gillham, J. Appl. Polym. Sci. 41 (1990) 2885.
[4] M. Cassettari, G. Salvetti, E. Tombari, S. Veronesi, G.P. Johari, J. Polym. Sci. B: Polym. Phys. 31 (1993) 119.
[5] H. Gobrecht, K. Hamann, G. Willers, J. Phys. E: Sci. Instrum. 4 (1971) 21.
[6] M. Cassettari, G. Salvetti, E. Tombari, S. Veronesi, G.P. Johari, Il Nuovo Cimento 14D (1992) 763.
[7] M. Cassettari, F. Papucci, G. Salvetti, E. Tombari, S. Veronesi, G.P. Johari, Rev. Sci. Instrum. 64 (1993) 1076.
[8] G. Van Assche, A. Van Hemelrijck, H. Rahier, B. Van Mele, Thermochim. Acta 268 (1995) 121.
[9] G. Van Assche, A. Van Hemelrijck, H. Rahier, B. Van Mele, Thermochim. Acta 304/305 (1997) 317.
[10] C. Ferrari, G. Salvetti, E. Tombari, G.P. Johari, Phys. Rev. E 54 (1996) R1058.
[11] C. Ferrari, G. Salvetti, E. Tognoni, E. Tombari, J. Thermal Anal. 47 (1996) 75.
[12] S. Montserrat, I. Cima, Thermochim. Acta 330 (1999) 189.
[13] I. Alig, W. Jenninger, J.E.K. Schawe, Thermochim. Acta 330 (1999) 167.
[14] J.E.K. Schawe, W. Winter, Thermochim. Acta 297 (1997) 9.
[15] S. Weyer, A. Hensel, C. Schick, Thermochim. Acta 304/305 (1997) 267.
[16] A.A. Lacey, C. Nikolopoulos, M. Reading, J. Thermal Anal. 50 (1997) 279.
[17] G.W.H. Höhne, H.K. Cammenga, W. Eysel, E. Gmelin, W. Hemminger, Thermochim. Acta 160 (1990) 1.
[18] H.K. Cammenga, W. Eysel, E. Gmelin, W. Hemminger, G.W.H. Höhne, S.M. Sarge, Thermochim. Acta 219 (1993) 333.

[19] G. Widmann, R. Riesen, Thermal Analysis, Hüthing, Heidelberg, 1987.
[20] B. Wunderlich, Y. Jin, A. Boller, Thermochim. Acta 238 (1994) 277.
[21] Y.H. Jeong, I.K. Moon, Phys. Rev. B 52 (1995) 6381.
[22] J.E.K. Schawe, J. Polym. Sci. B: Polym. Phys. 36 (1998) 2165.
[23] J.E.K. Schawe, S. Theobald, J. Non-Cryst. Solids 235–237 (1998) 496.
[24] C. Schick, M. Merzlyakov, A. Hensel, J. Chem. Phys. 111 (1999) 2695.
[25] J.E.K. Schawe, Thermochim. Acta 304/305 (1997) 111.
[26] J.E.K. Schawe, G.W.H. Höhne, Thermochim. Acta 287 (1996) 213.
[27] S. Vyazovkin, Thermochim. Acta 236 (1994) 1.
[28] I. Alig, W. Jenninger, J. Polym. Sci. B: Polym. Phys. 36 (1998) 2461.